

# Leptophilic Dark Matter with $Z'$ interactions

Nicole F. Bell,<sup>1</sup> Yi Cai,<sup>1</sup> Rebecca K. Leane,<sup>1</sup> and Anibal D. Medina<sup>1</sup>

<sup>1</sup>*ARC Centre of Excellence for Particle Physics at the Terascale  
School of Physics, The University of Melbourne, Victoria 3010, Australia*

(Dated: July 14, 2014)

We consider a scenario where dark matter (DM) interacts exclusively with Standard Model (SM) leptons at tree level. Due to the absence of tree-level couplings to quarks, the constraints on leptophilic dark matter arising from direct detection and hadron collider experiments are weaker than those for a generic WIMP. We study a simple model in which interactions of DM with SM leptons are mediated by a leptophilic  $Z'$  boson, and determine constraints on this scenario arising from relic density, direct detection, and other experiments. We then determine current LHC limits and project the future discovery reach. We show that, despite the absence of direct interactions with quarks, this scenario can be strongly constrained.

## I. INTRODUCTION

The identity of dark matter (DM), thought to make up approximately 25 percent of the energy-matter content of the universe [1–3], has remained elusive since it was first suggested over 80 years ago. Although there are an abundance of proposed particle physics models which can potentially account for dark matter, the most well studied class of model is that involving a weakly interacting massive particle (WIMP). WIMPs are appealing dark matter candidates because they can naturally account for the dark matter relic abundance via the “WIMP miracle” [2], while also offering realistic prospects for detection in a variety of direct detection, collider, and indirect detection experiments.

However, the non-observation of WIMPs thus far has begun to place meaningful constraints on the WIMP parameter space. Experiments at the LHC, which is a proton-proton collider, have not identified a DM signal. Direct detection (DD) experiments, which require nucleon-DM interactions, similarly do not report a DM signal and are placing tough limits on DM-nucleon cross-sections [4, 5], approaching the neutrino wall. However, the exclusions from these experiments are based on DM-hadron interactions, perhaps hinting that either the DM does not interact in such a way, or such interactions are suppressed. To relax constraints on the DM parameter space, we shall consider an alternate framework where direct DM-hadron interactions do not occur, and instead the DM couples exclusively to SM leptons at tree level. This is referred to as leptophilic dark matter (LDM) [6–22].

A leptophilic DM model may be tested via the three usual DM searches: direct detection, indirect detection and collider searches. However, the phenomenology of leptophilic DM is quite different to that of a generic WIMP. Although leptophilic DM does not couple to quarks at tree-level, such couplings will inevitably exist at higher order. DM detection processes involving quarks will thus still yield limits, though they will be relaxed by the presence of loop factors and/or additional coupling constants, thereby increasing the allowed parameter

space. For example, there exists a loop-suppressed direct detection process shown in Fig. 1 [20]. We shall see that despite the suppressed nature of this process, direct detection still places meaningful constraints on leptophilic dark matter.

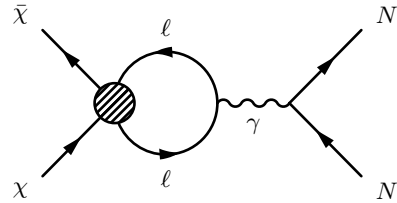


FIG. 1. Loop-suppressed direct detection signal for leptophilic dark matter.

Indirect detection experiments are a scan of the astrophysical sky, searching for unexplained fluxes which may be produced as a result of DM annihilation or decay. For low DM masses, interesting indirect detection bounds have been placed using Fermi observations of dwarf spheroidal galaxies [23]. At higher DM masses, significant interest in leptophilic DM was sparked by an excess in the cosmic ray positron fraction measured by the PAMELA [24], Fermi [25] and AMS [26] experiments. Given that no corresponding antiproton excess was seen, this suggested models in which DM annihilates, with a large cross section, to leptonic final states. However, these signals are subject to significant astrophysical uncertainties, and may in fact be produced by nearby pulsars [27, 28]. Moreover, as noted above, a model can only be “leptophilic” at lowest order with higher order process inevitably producing hadrons with non-negligible fluxes [29]. In this work, we shall not attempt to explain the positron results, but instead focus on LHC and direct detection bounds on leptophilic dark matter.

Collider searches at the LHC and LEP [10, 30] have placed interesting limits on standard WIMPs. The most generic, model independent limits are those obtained from the mono-X searches [31–37] (mono-jet, mono-photon or mono-W/Z). These signals are obtained when a single SM particle recoils against missing momentum,

attributed to dark matter particles which escape undetected. However, the mono-X searches at the LHC require that dark matter to couple to quarks, and are thus not applicable for a leptophilic scenario. There exist mono-photon limits from LEP [30], however these are only relevant for DM coupling to electrons (rather than muons or taus) and only extend to low DM masses. The LHC collider signals for leptophilic DM are very different from the mono-X signals and will be discussed in section VI below in the context of our example model.

The outline of the paper is as follows: We introduce a simple leptophilic model in Section II, consider relic density requirements in Section III, and discuss direct detection and other constraints in Section IV and V respectively. The LHC collider phenomenology for leptophilic dark matter is discussed in Section VI, and our main results are summarized in Fig. 5, 13, 14 and 15.

## II. LEPTOPHILIC MODEL

To fully investigate a LDM scenario, we shall adopt a particular simple model. We introduce a new spin-1 vector boson,  $Z'$ , which mediates interactions between SM leptons and the DM. Such a setup can be described via the Lagrangian

$$\begin{aligned} \mathcal{L} = & \mathcal{L}_{SM} - \frac{1}{4} Z'_{\mu\nu} Z'^{\mu\nu} - \frac{\epsilon}{2} Z'_{\mu\nu} B^{\mu\nu} + i\bar{\chi}\gamma_\mu\partial^\mu\chi \quad (1) \\ & + \bar{\chi}\gamma^\mu(g_\chi^V + g_\chi^A\gamma^5)\chi Z'_\mu + \bar{\ell}\gamma^\mu(g_\ell^V + g_\ell^A\gamma^5)\ell Z'_\mu \\ & - m_\chi\bar{\chi}\chi + \frac{1}{2}m_{Z'}^2 Z'_\mu Z'^\mu, \end{aligned}$$

where  $\epsilon$  is the kinetic mixing parameter of  $Z'$  and SM hypercharge gauge boson,  $\ell = e, \mu, \tau, \nu_e, \nu_\mu, \nu_\tau$  are the SM leptons,  $g_\ell = g_e, g_\mu, g_\tau$  are the  $Z'$  coupling strengths to each SM lepton flavor, and  $g_\chi$  is the coupling strength of the  $Z'$  to DM. We allow both vector (V) and axial-vector (A) couplings of the  $Z'$ . The parameters to investigate, therefore, are  $g_\chi, g_\ell, m_{Z'}, m_\chi$ , along with relevant cross sections. In this general setup, a mass generation mechanism for the  $Z'$  and DM is not specified.

At low energies, such as those relevant for direct detection, the  $Z'$  interactions can be well approximated by an effective contact operator,

$$\mathcal{L}_{eff} = \frac{1}{\Lambda^2}(\bar{\chi}\Gamma_\chi\chi)(\bar{\ell}\Gamma_\ell\ell), \quad (2)$$

where the effective cut-off scale is

$$\Lambda = \frac{m_{Z'}}{\sqrt{g_\chi g_\ell}}. \quad (3)$$

Given the form of the  $Z'$  interactions in Eq. 1, the possible Lorentz structures are combinations of vector (V) and axial-vector (A) bilinears:  $\Gamma_\chi \otimes \Gamma_\ell = V \otimes V, A \otimes V, V \otimes A$  or  $A \otimes A$ . However, in order to permit SM Yukawa couplings without breaking  $U(1)_L$  gauge invariance, the  $Z'$  coupling to the SM leptons must be vectorlike, thus

we shall require  $\Gamma_\ell = V$ . We list the possible Lorentz structures in Table I, and summarise their pertinent features.

TABLE I. Lorentz structure of the  $Z'$  couplings. For axial vector couplings to leptons, the loop-level direct detection signal vanishes [20]. However, in order for the SM Yukawa couplings to respect  $U(1)_L$  gauge invariance, the  $Z'$  couplings to leptons should be vectorlike. Also note that  $\Gamma_\chi = V$  is not permitted for Majorana DM.

$\Gamma_\chi \otimes \Gamma_\ell$	$\sigma(\chi\chi \rightarrow \bar{\ell}\ell)$	$\sigma(\chi N \rightarrow \chi N)$	Gauge invariant?
$V \otimes V$	$s$ -wave	1 (1-loop)	Yes
$A \otimes V$	$p$ -wave	$v^2$ (1-loop)	Yes
$V \otimes A$	$s$ -wave	-	No
$A \otimes A$	$p$ -wave	-	No

There has been some previous work on vector bosons which couple only to leptons. Considering only SM fields, the symmetries  $U(1)_{L_i-L_j}$  are anomaly free and can thus be gauged [38–40]; models in which DM interacts via a  $L_\mu - L_\tau$  gauge boson have recently been explored in [17, 21, 41]. We take a different approach in the present work and consider a leptophilic  $Z'$  which couples to a single lepton flavor, taking each flavour in turn. Phenomenologically, this is a natural choice because the experimental constraints depend on which lepton flavor is being considered. With this approach, new dark sector particles must be chosen with the correct quantum numbers to cancel anomalies. However, any hidden sector particles other than the DM candidate can be taken to be heavy enough to be decoupled from our Lagrangian, while light enough to still contribute to anomaly cancellation. We thus take the coupling strengths  $g_\ell^V$  and  $g_\chi^{A,V}$  as free parameters to be constrained.

## III. DARK MATTER RELIC DENSITY

In our leptophilic framework the dominant DM annihilation channels are

$$\chi\bar{\chi} \rightarrow \ell^-\ell^+, \bar{\nu}_\ell\nu_\ell, Z'Z', \quad (4)$$

with the corresponding Feynman diagrams shown in Fig. 2. To determine the parameter space allowed by relic density constraints, we implemented our model with FeynRules [42] and generated model files for MicroMEGAs [43] for the relic density calculation. We then performed a scan over  $m_{Z'}, m_\chi, g_\ell, g_\chi$  to determine the parameters which yield the correct relic density,  $\Omega_\chi h^2 = 0.1187 \pm 0.0017$  [44].

In Fig. 5, 13, 15, we plot relic density curves in the  $g_\ell = g_\chi$  vs  $m_{Z'}$  plane, for various choices of the DM mass, and in Fig. 14 for  $4g_\mu = g_\chi$  and  $8g_\mu = g_\chi$ . Parameters must lie on these curves to produce the correct

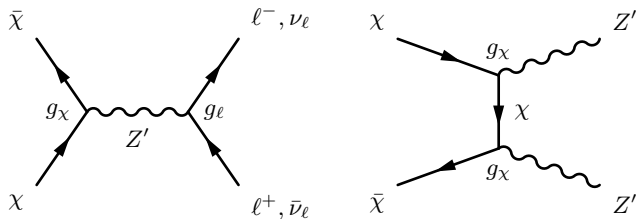


FIG. 2. DM annihilation processes, which determine the relic density at freezeout.

relic density. Larger values of the couplings would lead to a subdominant contribution to the relic density, while smaller couplings would overclose the universe unless additional annihilation channels were present.

The features of the relic density curves can be easily understood: The  $Z'Z'$  channel is kinematically open only for  $m_{Z'} < m_\chi$ , while for  $m_{Z'} > m_\chi$  the freeze-out is determined by annihilation to leptons. The annihilation cross section to leptons has an  $s$ -wave contribution when  $\Gamma_\chi = V$ , but proceeds via a velocity suppressed  $p$ -wave contribution when  $\Gamma_\chi = A$ . Resonant production of DM occurs when  $m_{Z'} \approx 2m_\chi$ , seen as strong dips in the relic density curves.

#### IV. DIRECT DETECTION

Direct detection experiments measure the recoil energy of SM nuclei after DM scattering. There are two ways leptophilic DM can be found at DD experiments: scattering at tree-level with electrons (particularly for experiments which do not veto leptonic recoils (i.e. DAMA/LIBRA)), or at higher orders with quarks. For tree-level scattering, the DM will scatter with electrons bound to atoms, causing electrons to absorb the recoil energy and eject from the atom, or remain bound to the atom but with increased energies and recoiled nuclei. It turns out this electron scattering is not very energetic, so that it cannot usually be seen at DD experiments. In the rare case the electron has a high enough initial momentum to produce a sufficiently energetic DD signal, the cross section suffers from large wavefunction suppression. Because of this, loop suppressed scattering with quarks will typically dominate DD for leptophilic DM [20] provided the diagrams do not vanish. The dominant loop level process for direct detection in our  $Z'$  model is shown in Fig. 3. A similar diagram in which the photon is replaced by a  $Z$  makes a negligible contribution.

The loop suppressed contributions to the DD cross section were calculated in the effective operator framework in Ref. [20]. For the Lorentz structures  $\Gamma_\chi \otimes \Gamma_\ell = A \otimes A$  and  $V \otimes A$ , the diagram in Fig. 1 vanishes, and thus direct detection provides no constraint. However, these Lorentz structures are not interesting for our model, because we require  $\Gamma_\ell = V$  in order for the SM Yukawa couplings to respect  $U(1)_L$  gauge invariance. For the remaining pos-

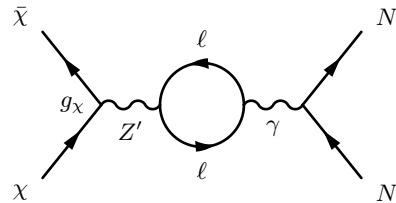


FIG. 3. Dominant direct detection process with a leptophilic  $Z'$  as SM-DM mediator.

sibilities,  $\Gamma_\chi \otimes \Gamma_\ell = V \otimes V$  and  $A \otimes V$ , the DM-nucleus cross sections are given by

$$\sigma_{VV} = \frac{\mu_N^2}{9\pi} \left[ \frac{\alpha_{EM} Z}{\pi \Lambda^2} \log \left( \frac{m_\ell^2}{\mu^2} \right) \right]^2, \quad (5)$$

$$\sigma_{AV} = \frac{\mu_N^2 v_\chi^2}{9\pi} \left( 1 + \frac{\mu_N^2}{2m_N^2} \right) \left[ \frac{\alpha_{EM} Z}{\pi \Lambda^2} \log \left( \frac{m_\ell^2}{\mu^2} \right) \right]^2, \quad (6)$$

where  $v_\chi^2 \approx 10^{-6}$  is the DM velocity,  $m_N$  and  $Z$  are the target nucleus' mass and charge respectively,  $\mu_N = m_N m_\chi / (m_N + m_\chi)$  is the reduced mass of the DM-nucleus system and  $\mu$  is the renormalization scale. As in [20] we set  $\mu = \Lambda$ .<sup>1</sup>

To compare these cross sections with results from a given direct detection experiment, we divide Eq. 5, 6 by the squared atomic mass number  $A^2$  to obtain the cross section per nucleon. The most stringent DD results are currently provided by the LUX experiment [5], for which  $A = 121$  (Xenon). In Fig. 4 we plot the constraints from the LUX experiment, in the  $m_\chi$ - $\Lambda$  plane, for both  $\Gamma_\chi \otimes \Gamma_\ell = V \otimes V$  and  $A \otimes V$ .

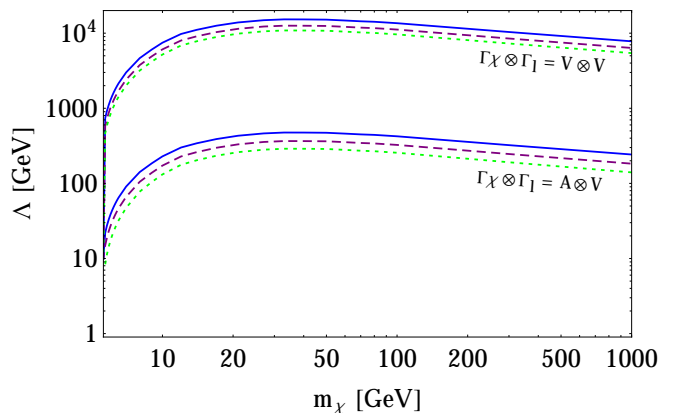


FIG. 4. Lower bounds on the cutoff,  $\Lambda$ , for fermionic DM coupling to leptons via a four-fermion effective contact operator, using exclusion limits from LUX. Limits are shown for electrons (solid, blue), muons (dashed, purple) and taus (dotted, green) for both  $\Gamma_\chi \otimes \Gamma_\ell = A \otimes V$  and  $V \otimes V$ . We see that the cutoff required for  $V \otimes V$  is much higher than that for  $A \otimes V$ .

<sup>1</sup> As the cross sections depend only logarithmically on  $\mu$ , extreme choices for this parameter can change the limits on  $g_{\ell,\chi}$  by at most a factor of a few.

As seen in Fig. 4, the direct detection bounds are considerably more stringent for the  $\Gamma_\chi \otimes \Gamma_\ell = V \otimes V$  case than for  $\Gamma_\chi \otimes \Gamma_\ell = A \otimes V$ . This is because the DD cross section for the later is suppressed by a factor of  $v_\chi^2$ . The DD and relic density constraints are compared in Fig. 5 for  $\Gamma_\chi \otimes \Gamma_\ell = V \otimes V$  and in Fig. 13, 14, 15 for  $\Gamma_\chi \otimes \Gamma_\ell = A \otimes V$ . For  $V \otimes V$ , the DD bound excludes all the parameter space for which the relic density constraint is satisfied, except if there is a very strong resonant enhancement of the annihilation cross section at  $m_\chi = 2m_{Z'}$ . In fact, the DD bounds on the  $V \otimes V$  case are much stronger than collider bounds and other constraints. In comparison, we see that more parameter space is open for  $A \otimes V$ , however, even in this case the DD experiments place non-trivial constraints.

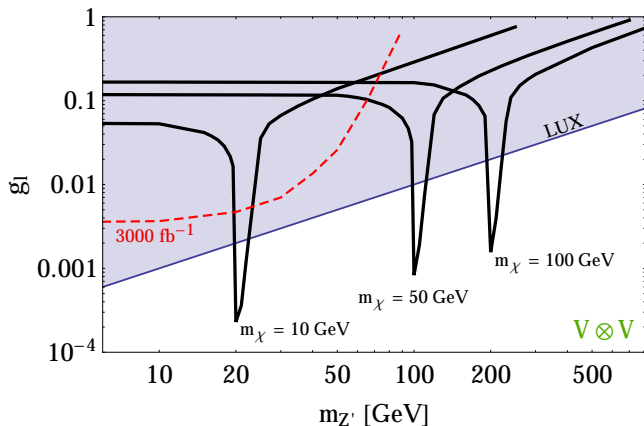


FIG. 5. Constraints on the  $g_\ell = g_\chi$  and  $m_{Z'}$  parameter space when  $\Gamma_\chi \otimes \Gamma_\ell = V \otimes V$ . The relic density curves are shown for  $m_\chi = 10, 50,$  and  $100$  GeV (black, solid), while the shaded region is excluded by the LUX direct detection results (for  $m_\chi = 20 - 100$  GeV). Also shown is the approximate future LHC reach at  $\sqrt{s} = 14$  TeV (see section VI) for coupling to  $e$  or  $\mu$ . It is clear that, for a  $\Gamma_\chi \otimes \Gamma_\ell = V \otimes V$  operator, the current direct detection results already exclude most of the parameter space for which the correct relic density is obtained.

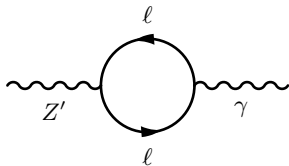


FIG. 6. Kinetic mixing of the  $Z'$  and SM photon.

In calculating the direct detection bounds, we have assumed the DM-nucleus cross section arises entirely from the loop diagram of Fig. 3. However, kinetic mixing of the  $Z'$  with the SM hypercharge  $Z'$  gauge boson (the  $\epsilon$  term in Eq. 1) would also make a contribution to the direct detection cross section. In fact, such a term should be present in the Lagrangian as it will be generated by loop diagrams such as that in Fig. 6. This loop contri-

bution to the kinetic mixing may be estimated as [45]

$$\epsilon = \frac{g_Y g_\ell}{16\pi^2} \log\left(\frac{\mu^2}{m_\ell^2}\right), \quad (7)$$

where  $\mu$  is a renormalization scale, and clearly leads to the same DD cross sections as those in Eq. 5 and Eq. 6. Using Eq. 7, we may translate our DD bounds into a constraint on the kinetic mixing parameter of  $\epsilon \lesssim \mathcal{O}(10^{-3}) - \mathcal{O}(10^{-4})$ . These direct detection bounds on  $\epsilon$  are more stringent than those arising from precision electroweak measurements, which require only  $\epsilon \lesssim \mathcal{O}(10^{-2})$  [46, 47].

Note that our DD cross sections should actually be considered naturalness estimates, in the case that the kinetic mixing is generated by the loop diagrams alone. More generally,  $\epsilon$  is a free parameter which runs with scale. In principle, the direct detection signal could be suppressed if  $\epsilon$  happened to run to a very small value at low scale. We regard this as unnatural, as it would involve a fine-tuned cancellation of the contribution of the loop diagram with a bare term in the Lagrangian. However, it is important to appreciate that the DD limits are not watertight constraints, but simply naturalness bounds.

## V. CONSTRAINTS FROM $(g-2)_\ell$ , LEP AND OTHER SEARCHES

We now outline further constraints on our scenario. Unlike the DD bounds, these additional limits depend sensitively on the lepton flavour. Measurements of  $(g-2)_\ell$  constrain the coupling of a  $Z'$  to each of the lepton flavours, resulting in a strong bound for the  $\mu$  flavour, and weaker bounds for  $e$  and  $\tau$ . Very stringent  $Z'$  bounds from LEP apply to the electron flavour alone, as do the LEP mono-photon bounds.

$(g-2)_\ell$ : A  $Z'$  which couples to leptons will make a contribution to the lepton anomalous magnetic dipole of [48]

$$\Delta(g-2)_\ell \sim \frac{g_\ell^2}{6\pi^2} \frac{m_\ell^2}{m_{Z'}^2}. \quad (8)$$

Upper limits on any additional contribution to  $(g-2)_\ell$  are  $4 \times 10^{-10}$ ,  $8 \times 10^{-9}$  and  $8 \times 10^{-2}$  for the electron, muon and tau respectively [49]. This requires the  $Z'$  coupling strengths to be

$$g_e \lesssim 0.3 \frac{m_{Z'}}{\text{GeV}}, \quad (9a)$$

$$g_\mu \lesssim 6 \times 10^{-3} \frac{m_{Z'}}{\text{GeV}}, \quad (9b)$$

$$g_\tau \lesssim \frac{m_{Z'}}{\text{GeV}}. \quad (9c)$$

**Neutrino scattering:** The Liquid Scintillator Neutrino Detector (LSND) measured the cross section for the elastic scattering process  $\nu_e + e^- \rightarrow \nu_e + e^-$ , placing a further constraint on the  $Z'$  coupling strength to electrons [50],

$$g_e \lesssim 3 \times 10^{-3} \frac{m_{Z'}}{\text{GeV}}. \quad (10)$$

This constraint is comparable to the LUX direct detection bound on  $g_e$  for the  $A \otimes V$  case.

**LEP-II  $Z'$  constraints:** The coupling of a  $Z'$  to electrons is constrained by results of the LEP-II experiments. For  $Z'$  masses greater than 209 GeV, the largest center-of-mass energy at which LEP operated, the constraints are expressed in terms of four-fermion contact operators, known as the compositeness bounds [51]. For a vector coupling to electrons this bound can be expressed as [51, 52]

$$g_e \lesssim 0.044 \times m_{Z'}/(200 \text{ GeV}). \quad (11)$$

For  $Z'$  masses below about 200 GeV, the four-fermion description is not valid, as the  $Z'$  mass is not large compared to the LEP beam energy, and resonant production is possible. A conservative limit can be taken as  $g \lesssim 0.04$  for  $m_{Z'} \lesssim 200$  GeV. Much stronger limits should hold for a  $Z'$  mass close to one of the centre of mass energies at which LEP ran, however no detailed analysis exists.

**LEP-II mono-photon constraints:** Monophoton searches at LEP-II place bounds on the couplings [30], which again are relevant only when the  $Z'$  couples to electrons. These constraints depend sensitively on the  $Z'$  decay width and thus on the ratio  $g_e/g_\chi$ . If we assume  $g_e \simeq g_\chi$ , then for  $m_\chi \lesssim m_{Z'}/2$  and  $m_{Z'} \gtrsim 30$  GeV these constraints are stronger than LUX, but are comparable to the LEP  $Z'$  bounds. For masses outside of this range, LUX is more constraining.

**Electroweak Precision Measurements:** In addition to the limits on kinetic mixing as discussed in section II, there are constraints on the ratio of the decay width of a  $Z'$  which couples to electrons and  $m_{Z'}$  from precision measurements of the line shape of the  $Z^0$  [46, 47]. However they do not constrain the  $g_e - m_{Z'}$  parameter space any further than the limits listed above.

## VI. LHC PHENOMENOLOGY

We now consider the LHC phenomenology for a leptophilic  $Z'$ . Because the  $Z'$  does not couple directly to quarks, the lowest order  $Z'$  production process is  $pp \rightarrow \ell^+ \ell^- Z'$ , in which a  $Z'$  is radiated from a lepton in a Drell-Yan process, as shown Fig. 7. The  $Z'$  production cross section is shown in Fig. 8. The cross section is large when  $m_{Z'} < m_Z$ , because the process in Fig. 7 can proceed via an on-shell  $Z$ . For  $m_{Z'} > m_Z$ , however, the cross section falls rapidly with increasing  $Z'$  mass, such

that detecting a  $Z'$  with mass beyond about 500 GeV would be challenging.

The  $Z'$  decays either to DM (or neutrinos) or to charged leptons, resulting in a pair of opposite sign dileptons plus missing  $E_T$ , or two pairs of opposite sign dileptons, respectively. The 2-lepton plus missing  $E_T$  signal competes with substantial SM backgrounds, in particular from the process  $Z$ +jets, such that detection prospects are poor. However, the 4-lepton signal is very distinctive and is examined in detail below.

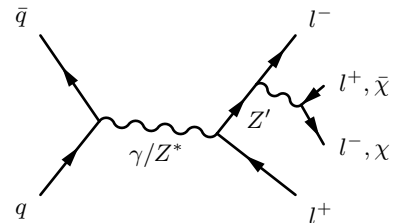


FIG. 7. Production of the  $Z'$  at a hadron collider. The  $Z'$  is radiated from a lepton in the Drell Yan process, and subsequently decays to either leptons or DM.

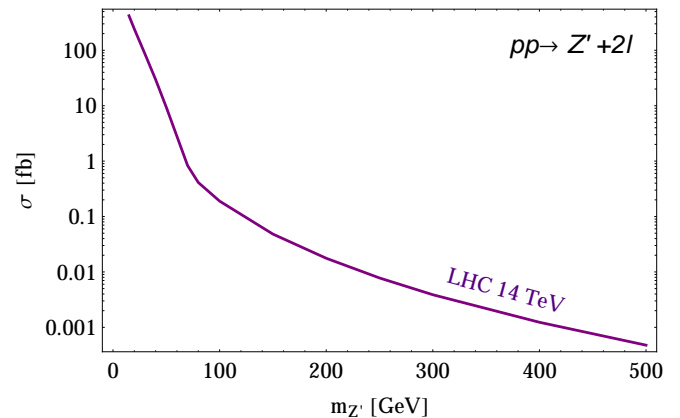


FIG. 8.  $Z'$  production cross section at the 14 TeV LHC, via the process  $pp \rightarrow \ell^+ \ell^- Z'$ . We have set  $g_\ell = 0.1$ .

The signal rates depend on the branching fraction of the  $Z'$  to charged leptons or DM, which depend on the mass and coupling strength of the  $Z'$ . For  $g_\chi = g_\ell$ , and in the limit  $m_{Z'} \gg m_\chi$ , we have

$$Br(Z' \rightarrow \ell\ell) = Br(Z' \rightarrow \chi\chi) = 2Br(Z' \rightarrow \nu_\ell\nu_\ell). \quad (12)$$

For other parameters, the branching ratios are evaluated numerically in our analysis.

### A. $Z'$ Decay to Leptons

We now consider the 4 lepton process,  $pp \rightarrow \ell^+ \ell^- Z' \rightarrow \ell^+ \ell^- \ell^+ \ell^-$ , in detail. The main SM backgrounds for this

process are

$$pp \rightarrow \ell^+ \ell^- Z \rightarrow \ell^+ \ell^- \ell^+ \ell^-, \quad (13a)$$

$$pp \rightarrow ZZ \rightarrow \ell^+ \ell^- \ell^+ \ell^-, \quad (13b)$$

with Eq. 13a making the dominant contribution. The  $pp \rightarrow 4\ell$  cross section has been measured at the  $Z$  resonance by the LHC experiments, ATLAS and CMS. The most constraining limits arise from the ATLAS analysis, which used an  $\sqrt{s} = 8$  TeV dataset at an integrated luminosity of  $20.7 \text{ fb}^{-1}$ , and measured the number of events to be consistent with the SM expectation. A similar analysis performed by CMS used only the  $\sqrt{s} = 7$  TeV data [53] and is less constraining. We reproduce the ATLAS analysis to find the current exclusion limits for our  $Z'$  model using the  $Z \rightarrow 4l$  search [54].<sup>2</sup> We also simulate events at  $\sqrt{s} = 14$  and higher luminosities, to project the future reach of the LHC.

To simulate our  $Z'$  signal and the relevant SM background, we implement our model with FeynRules [42], generate parton level events in MadGraph [55] and then interface with Pythia [56] to produce hadronic level events. For processes involving electrons, we also interface the Pythia output with the PGS detector simulation [57]. Finally, we use MadAnalysis [58] to analyse the events. We determine the significance according to

$$\sigma = N_{Z'}/\sqrt{N_{Z'} + N_{SM}}, \quad (14)$$

where  $N_{Z'}$  is the number of simulated events for the  $Z'$  model, and  $N_{SM}$  is the number of ATLAS events observed, which is consistent with the predicted number of SM events. Excluded parameters are those which have a deviation from the SM of  $\sigma \gtrsim 3.0$ . We neglect systematic uncertainties, as they are very low for our purely leptonic final states [54]. Given that the number of signal and background events are comparable, a small systematic uncertainty will not have a significant effect on the results.

We consider only the  $Z \rightarrow 4\mu$  and  $Z \rightarrow 4e$  part of the ATLAS analysis. Mixed flavour final states are not possible, because we assume the  $Z'$  couples to a single lepton flavour. For the case of the  $4\mu$  signal, we perform different analyses for low mass ( $m_{Z'} < m_Z$ ) and high mass ( $m_{Z'} > m_Z$ )  $Z'$  bosons. For the  $4e$  signal, however, we perform only the low mass analysis, as the LEP  $Z'$  searches already eliminate the high mass parameter space that could be probed at the LHC.

There is no available analysis for a four tau final state, as tau reconstruction is significantly more difficult and suffers a much lower efficiency than detecting  $\mu$  or  $e$ . Therefore, there are no current collider constraints which can be placed on a scenario in which the  $Z'$  couples only to the tau flavour.

<sup>2</sup> A similar analysis has been performed recently for the 4 muon final state in Refs. [59, 60].

### 1. Four Electron Final State: $m_{Z'} < m_Z$

We replicate the ATLAS  $pp \rightarrow 4e$  analysis at the  $Z$  resonance, for which the candidate events have two pairs of opposite sign electrons. The following selection cuts are made:

- $p_{T,e} > 7$  GeV and  $|\eta| < 2.47$  for individual electrons
- Candidate separation of  $\Delta R_{ee} > 0.1$
- $M_{e^-,e^+} > 20, 5$  GeV for the leading pair and next to leading pair in momentum
- $p_{T,e} > 20, 15, 10$  GeV for the leading three electrons
- Invariant mass of electron quadruplet is restricted to events near the  $Z$  resonance:  $80 < M_{4e} < 100$  GeV

For the four electron case, the hadronic level events generated by Pythia [56] are interfaced with the PGS detector simulator before being interfaced to MadAnalysis at reconstruction level [58]. This is necessary for electrons, as they are reconstructed from energy clusters in an electromagnetic calorimeter, which are matched to reconstructed electron tracks in the inner detector [61], for which detector effects and efficiencies are not negligible. With this procedure, our simulated number of SM events was consistent with that measured by ATLAS.

The current ATLAS exclusion based on the  $4e$  process at  $20.7 \text{ fb}^{-1}$  is shown in Fig. 15, assuming  $g_\ell = g_\chi$ . We also show future discovery curves at the higher luminosities of 300 and  $3000 \text{ fb}^{-1}$ .

### 2. Four Muon Final State: $m_{Z'} < m_Z$

We replicate the ATLAS  $pp \rightarrow 4\mu$  analysis at the  $Z$  resonance, for which the candidate events have two pairs of opposite sign muons. The following selection cuts are made:

- $p_{T,\mu} > 4$  GeV and  $|\eta| < 2.7$  for individual muons
- Candidate separation of  $\Delta R_{\mu\mu} > 0.1$
- $M_{\mu^-, \mu^+} > 20, 5$  GeV for the leading pair and next to leading pair in momentum
- $p_{T,\mu} > 20, 15, 8$  GeV for the leading three muons
- Invariant mass of muon quadruplet is restricted to events near the  $Z$  resonance:  $80 < M_{4\mu} < 100$  GeV

We do not perform a detector simulation for the  $pp \rightarrow 4\mu$  analysis, as detection efficiencies are very high and the small smearing of data due to detector effects has a negligible effect on our results.

The current ATLAS exclusion based on the  $4\mu$  process at  $20.7 \text{ fb}^{-1}$  is shown in Fig. 15, assuming  $g_\ell = g_\chi$ . We

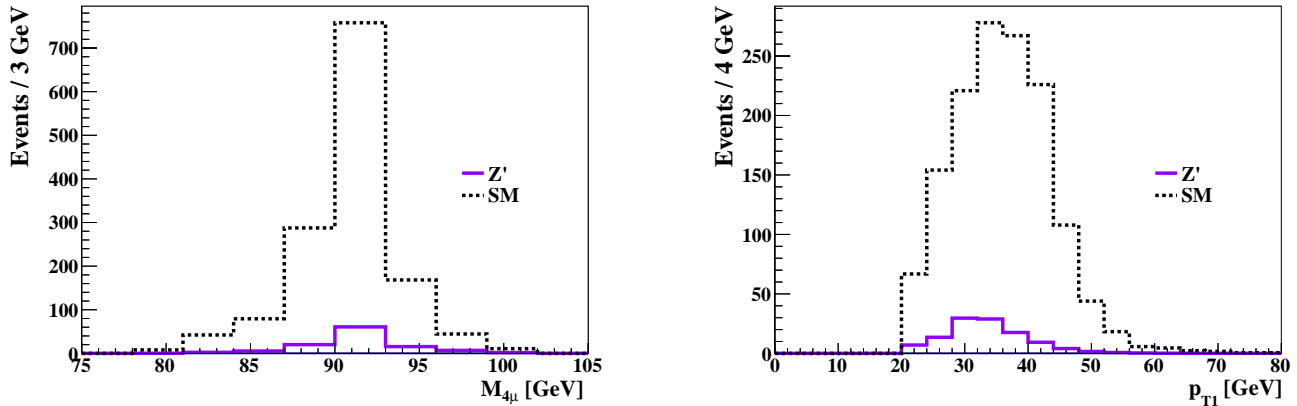


FIG. 9. Invariant mass for four muons (left) and transverse momentum  $p_T$  for leading in  $p_T$  muon (right) for  $pp \rightarrow 4\mu$  in the SM and  $Z'$  model (with  $m_{Z'} = 60$  GeV,  $m_\chi = 10$  GeV,  $g_\mu = g_\chi = 0.1$ ), at  $\sqrt{s} = 14$  TeV and  $\mathcal{L} = 300$   $fb^{-1}$ . The peak in the four muon invariant mass spectrum is a reconstruction of the  $Z$  mass.

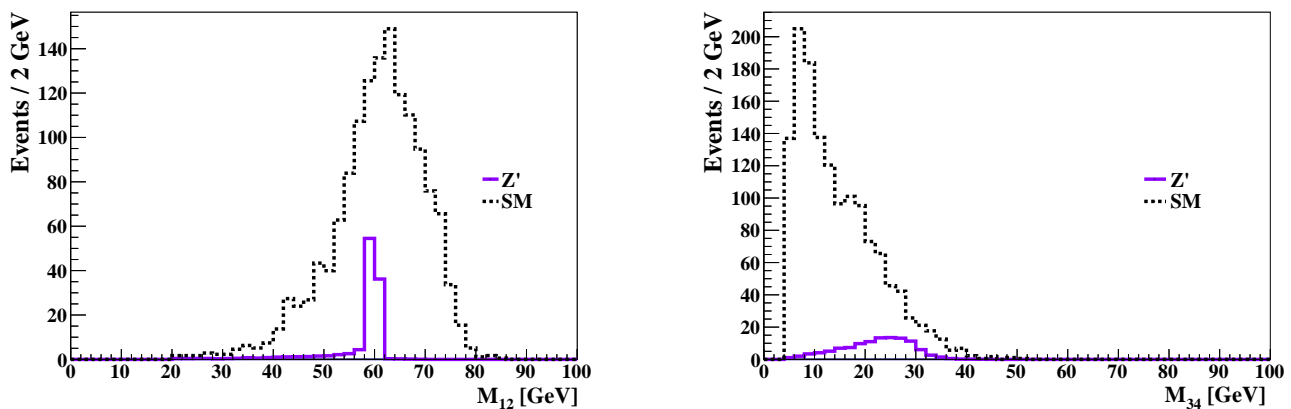


FIG. 10. Invariant mass for first and second leading muons in  $p_T$  (left) and third and fourth leading muons in  $p_T$  (right) for  $pp \rightarrow 4\mu$  in the SM and  $Z'$  model (with  $m_{Z'} = 60$  GeV,  $m_\chi = 10$  GeV,  $g_\mu = g_\chi = 0.1$ ), at  $\sqrt{s} = 14$  TeV and  $\mathcal{L} = 300$   $fb^{-1}$ . The mass of the  $Z'$  can be seen clearly as the resonance at  $m_{Z'} = 60$  GeV in the invariant mass spectrum  $M_{12}$ .

also show future discovery curves at the higher luminosities of 300 and 3000  $fb^{-1}$ . We show a selection of kinematic plots in Fig. 9, 10 for an example choice of parameters:  $m_{Z'} = 60$  GeV,  $m_\chi = 10$  GeV,  $g_\mu = g_\chi = 0.1$ . (The relevant  $Z'$  branching fractions are  $Br(\mu^+\mu^-) = 0.428$ ,  $Br(\bar{\nu}_\mu\nu_\mu) = 0.214$  and  $Br(\bar{\chi}\chi) = 0.358$ .) These parameters are allowed by the  $\sqrt{s} = 8$  TeV ATLAS results, but sit on the  $3\sigma$  curve corresponding to  $\mathcal{L} = 300$   $fb^{-1}$  at  $\sqrt{s} = 14$  TeV, and thus can be discovered or ruled out with future LHC data.

Note that the choice of  $g_\chi$  affects the cross section by controlling the relative sizes of the  $Z'$  branching ratios to lepton or dark matter final states. We can weaken constraints from the four muon search by increasing the  $Z'$  coupling strength to dark matter, with results for  $4g_\mu = g_\chi$  and  $8g_\mu = g_\chi$  shown in Fig. 14.

### 3. Four Muon Final State: $m_{Z'} > m_Z$

We now consider higher  $Z'$  masses than those probed by the 4 lepton search at the  $Z$  resonance, i.e.,  $m_{Z'} > m_Z$ . The  $Z'$  production via the diagram in Fig. 7 now proceeds via an off-shell  $Z^*$ , with a much lower cross section as seen in Fig. 8. We perform a similar analysis to that described in the previous section, with appropriate changes tailored to this higher mass case. Specifically, we remove the cut on the 4 muon invariant mass, so that we are no longer restricted to events near the  $Z$ -resonance, and place cuts on the di-muon invariant masses to remove the  $Z$ -peak (arising from processes in which the  $Z'$  in Fig. 7 is replaced by a SM  $Z$ ).

We implement the following selection cuts:

- $p_{T,\mu} > 4$  GeV and  $|\eta| < 2.7$  for individual muons
- Candidate separation of  $\Delta R_{\mu\mu} > 0.1$

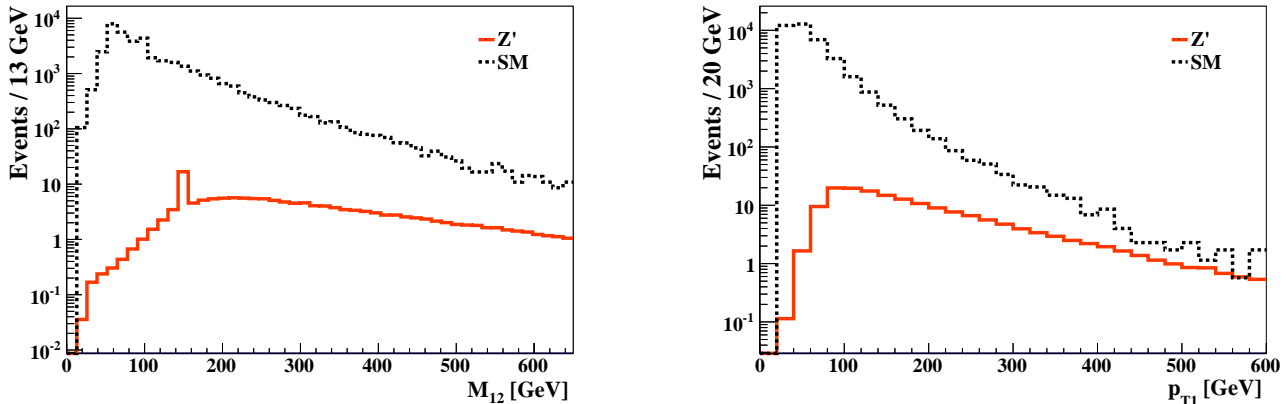


FIG. 11. Invariant mass for first and second leading muons in  $p_T$  (left) and transverse momentum  $p_T$  for  $p_T$  leading muon (right) both before cuts, for  $pp \rightarrow 4\mu$  in the SM and  $Z'$  model (with  $m_{Z'} = 150$  GeV,  $m_\chi = 10$  GeV,  $g_\mu = g_\chi = 0.19$ ), at  $\sqrt{s} = 14$  TeV and  $\mathcal{L} = 3000$   $fb^{-1}$ .

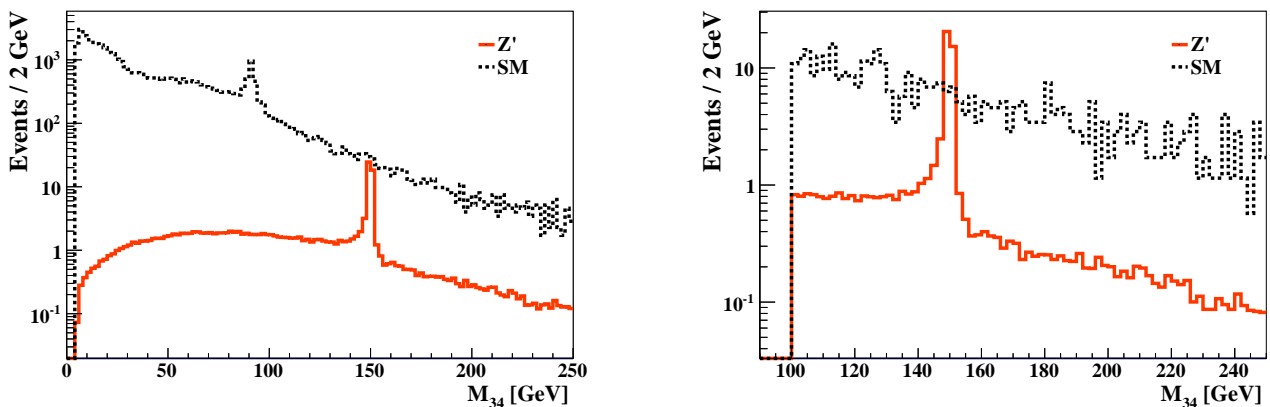


FIG. 12. Invariant mass of third and fourth leading in  $p_T$  muons before cuts (left) and after cuts (right), for  $pp \rightarrow 4\mu$  in the SM and  $Z'$  model (with  $m_{Z'} = 150$  GeV,  $m_\chi = 10$  GeV,  $g_\mu = g_\chi = 0.19$ ), at  $\sqrt{s} = 14$  TeV and  $\mathcal{L} = 3000$   $fb^{-1}$ .

- $M_{\mu^-, \mu^+} > 100$  GeV for both the leading pair and next to leading pair in momentum
- $p_{T, \mu} > 120, 100, 8$  GeV for the leading three muons

Due to the low cross sections, large luminosities are required to constrain the high  $Z'$  masses. In Fig. 13 we show the projected  $3\sigma$  exclusion curve at  $3000$   $fb^{-1}$ . Notice that in the high  $m_{Z'}$  searches at high luminosities one is able to probe  $Z'$ -masses up to  $m_{Z'} \sim 500$  GeV. We show a selection of kinematic plots in Fig. 11, 12 for an example choice of parameters ( $m_{Z'} = 150$  GeV,  $m_\chi = 10$  GeV,  $g_\mu = g_\chi = 0.28$ ) which fall on this curve. The effectiveness of the kinematic cuts can be seen by comparing the LH and RH panels of Fig. 12, which display the  $M_{34}$  distributions before and after cuts, respectively.

## B. $Z'$ Decay to Dark Matter

We now consider the process  $pp \rightarrow \ell\ell\chi\chi$  (see Fig. 7) for which the signal is a pair of opposite sign leptons plus missing  $E_T$ . Unlike the 4 lepton signal, the 2 lepton + missing  $E_T$  signal is subject to significant backgrounds, which render the detection prospects very poor. The dominant SM backgrounds arise from

$$pp \rightarrow Z + \text{jets} \rightarrow \ell^+\ell^- + \text{jets}, \quad (15a)$$

$$t\bar{t} \rightarrow b\bar{b}WW \rightarrow b\bar{b}\ell^+\ell^- \nu_\ell \bar{\nu}_\ell. \quad (15b)$$

The  $Z + \text{jets}$  background, with soft jets from the underlying QCD process, produces an enormous number of dileptons plus missing  $E_T$  events, where the missing energy arises from jet misidentification or energy mismeasurement. To overcome this background we would need to select events with  $E_T \gtrsim 200$  GeV. However, a



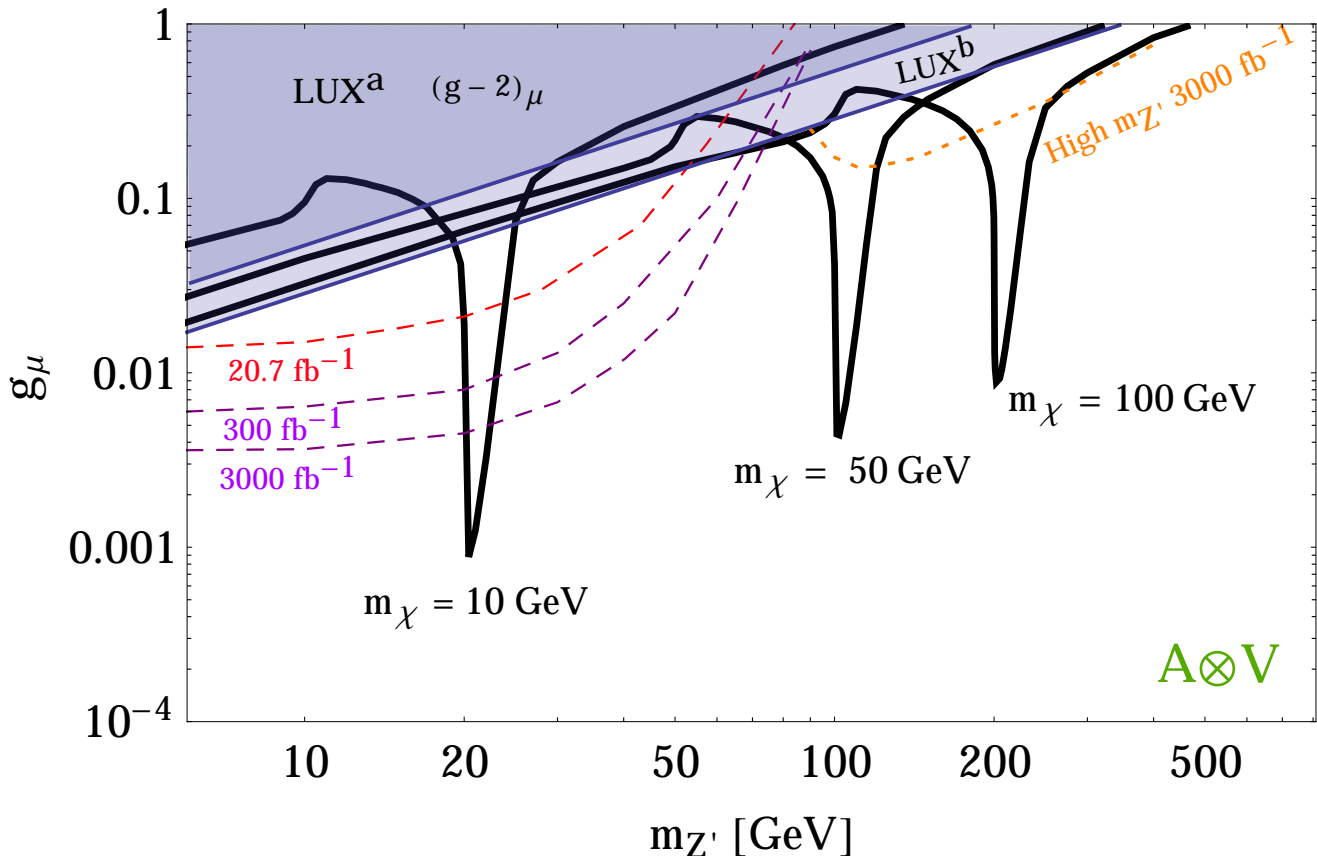


FIG. 13. Parameter space for  $g_\mu$  vs.  $m_{Z'}$  with  $g_\chi = g_\mu$ . Shown are excluded regions from  $(g-2)_\mu$ , as well as two excluded regions from LUX direct detection corresponding to two different DM mass ranges: LUX<sup>a</sup> is for approximately  $m_\chi = 10, 1000$  GeV and LUX<sup>b</sup> is for the range  $m_\chi = 20 - 100$  GeV. Exclusions from LUX<sup>a</sup> and  $(g-2)_\mu$  are overlapping in this plot. Relic density curves are shown in black for  $m_\chi = 10, 50, 100$  GeV. Dashed lines are ATLAS exclusions and reaches: top dashed curve is ruled out by ATLAS data at  $\sqrt{s} = 8$  TeV and  $\mathcal{L} = 20.7 fb^{-1}$ , middle is the ATLAS discovery reach at  $\sqrt{s} = 14$  TeV and  $\mathcal{L} = 300 fb^{-1}$ , and the bottom dashed curve is the ATLAS discovery reach at  $\sqrt{s} = 14$  TeV and  $\mathcal{L} = 3000 fb^{-1}$ . The dotted line shows the ATLAS reach at  $3000 fb^{-1}$  for a high mass  $Z'$ . The LHC limits all assume  $m_\chi = 10$  GeV.

signal in this range would require a  $Z'$  greater than 200 GeV, for which the production cross section is extremely small. Nonetheless, despite being unable to detect the DM production process, the presence of the  $Z'$  coupling to DM still affects the collider phenomenology through the  $Z'$  width and branching fractions, as can be seen by comparing Fig. 13 and 14. Finally, we note that this dilepton plus missing  $E_T$  signal could be a relevant discovery channel in a future lepton collider such as the ILC, where the  $Z$ +jets background is not present.

## VII. DISCUSSION

Our main results are summarized in Fig. 5 for  $\Gamma_\chi \otimes \Gamma_\ell = V \otimes V$  and Fig. 13, 14, 15 for  $\Gamma_\chi \otimes \Gamma_\ell = A \otimes V$ . Note that because  $V \otimes V$  is highly constrained by the direct detection results, we have explored the  $A \otimes V$  case in much greater detail.

In Fig. 13, we summarise the results for a  $Z'$  that couples to the muon flavour. We see that there is significant overlap of the excluded regions from  $(g-2)_\mu$  and direct detection results, which each place non-trivial constraints on the model. In particular, for values of  $m_\chi \lesssim 100$  GeV, they rule out those parameters for which the relic density can be explained, unless the masses fall in the vicinity of a resonance at  $m_{Z'} \sim 2m_\chi$ . The LHC results place complementary constraints. For a low mass  $Z'$  (those with  $m_{Z'} < m_Z$ ), the collider limits rule out smaller values of the coupling  $g_\ell$  than can be probed by DD or  $(g-2)$ . The projected limits (or discovery sensitivity) for the 14 TeV LHC at  $3000 fb^{-1}$  significantly covers the low  $m_{Z'}$  parameter space, even for parameters for which the DM relic density is controlled by resonant annihilation. For a higher mass  $Z'$  ( $m_{Z'} > m_Z$ ) the production cross section at the LHC is suppressed, and hence only the  $3000 fb^{-1}$  results are shown in the figure. It is clear that, for sufficiently large  $m_\chi$  or  $m_{Z'}$ , it will be possible to find pa-

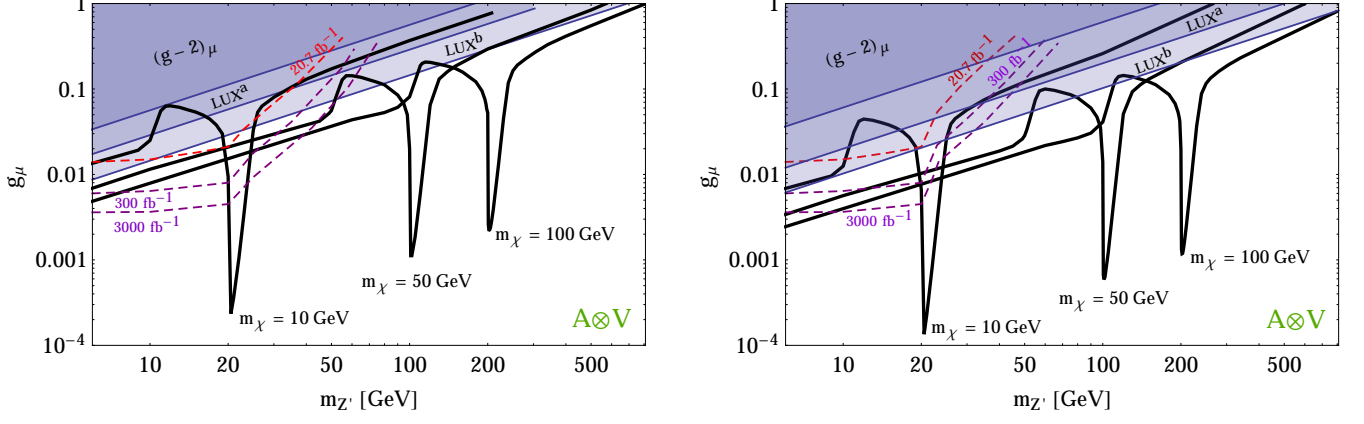


FIG. 14. Parameter space for  $g_\mu$  vs.  $m_{Z'}$ , where  $g_\chi = 4g_\mu$  (left) and  $g_\chi = 8g_\mu$  (right). Shown are excluded regions from  $(g-2)_\mu$ , and two excluded regions from LUX direct detection are shown corresponding to two different DM mass ranges: LUX<sup>a</sup> is for approximately  $m_\chi = 10, 1000$  GeV and LUX<sup>b</sup> is for the range  $m_\chi = 20 - 100$  GeV. Relic density curves are shown in black for  $m_\chi = 10, 50, 100$  GeV. Dashed lines are ATLAS exclusions and reaches: top is ruled out by ATLAS data at  $\sqrt{s} = 8$  TeV and  $\mathcal{L} = 20.7 fb^{-1}$ , middle is the ATLAS discovery reach at  $\sqrt{s} = 14$  TeV and  $\mathcal{L} = 300 fb^{-1}$ , and bottom is the ATLAS discovery reach at  $\sqrt{s} = 14$  TeV and  $\mathcal{L} = 3000 fb^{-1}$ . These exclusion/discovery curves are the same as for the  $g_\mu = g_\chi$  case when  $m_{Z'} < 2m_\chi$ . The LHC limits all assume  $m_\chi = 10$  GeV.

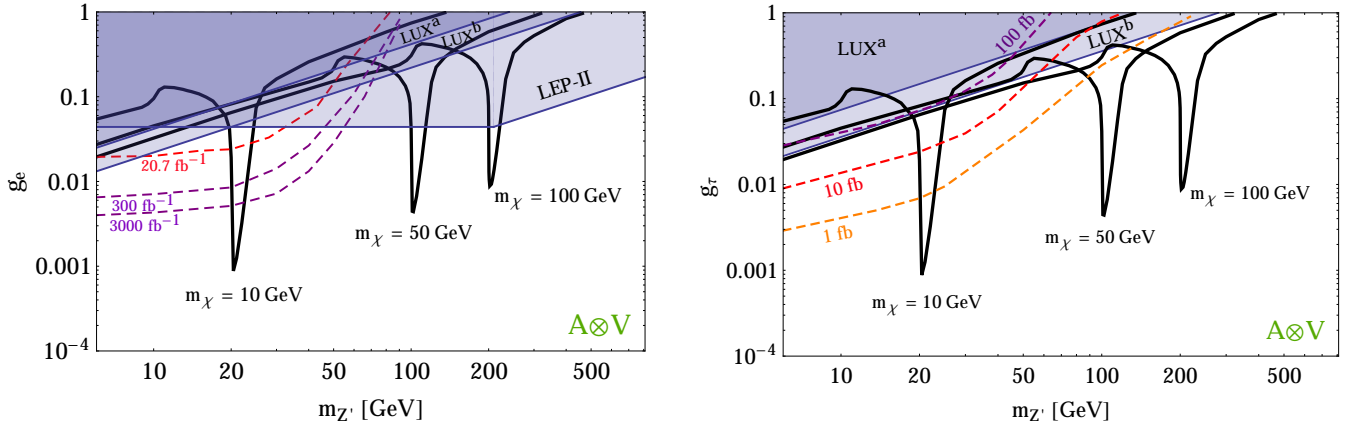


FIG. 15. Parameter space for  $g_e$  vs.  $m_{Z'}$  with  $g_\chi = g_e$  (left) and  $g_\tau$  vs.  $m_{Z'}$ , with  $g_\chi = g_\tau$  (right). Two excluded regions from LUX direct detection are shown corresponding to two different DM mass ranges: LUX<sup>a</sup> is for approximately  $m_\chi = 10, 1000$  GeV and LUX<sup>b</sup> is for the range  $m_\chi = 20 - 100$  GeV. Relic density curves are shown in black for  $m_\chi = 10, 50, 100$  GeV. Exclusions from LEP-II (electrons only) shown on the left. Dashed lines on the electron plot (left) are ATLAS exclusions and reaches: top is ruled out by ATLAS data at  $\sqrt{s} = 8$  TeV and  $\mathcal{L} = 20.7 fb^{-1}$ , middle is the ATLAS discovery reach at  $\sqrt{s} = 14$  TeV and  $\mathcal{L} = 300 fb^{-1}$ , and bottom is the ATLAS discovery reach at  $\sqrt{s} = 14$  TeV and  $\mathcal{L} = 3000 fb^{-1}$ . The LHC limits all assume  $m_\chi = 10$  GeV. For the tau plot (right), there are no collider limits due to low efficiencies for reconstructing a four tau final state. Instead, dashed lines show contours of  $Z'$  production cross sections of 1, 10 and 100 fb.

parameters which satisfy the relic density requirement and escape all constraints.

The constraints on a  $Z'$  which couples to the  $e$  flavour are shown in LH panel of Fig. 15. The DD constraints are similar for all flavours, as they depend only logarithmically on the lepton masses. For electrons, the  $(g-2)$  constraint is too weak to be shown on the plot. However, the  $e$ -flavour is subject to LEP-II  $Z'$  constraints, which are very strong and eliminate much parameter space that is open for the  $\mu$ -flavour. As a result, the relic density

constraints cannot be met unless one lives very close to a resonance.

Finally, we consider the  $\tau$  flavour in the RH panel of Fig. 15. Here the  $(g-2)$  constraints are again too weak to be shown on the plot. As we mentioned above, there are no current collider analyses for this case, due to the difficulties associated with tau reconstruction. Instead, we indicate in Fig. 15 the  $Z'$  production cross section, as a crude indication of the sensitivity that could be obtained were a dedicated analysis for the  $4\tau$  final state to be

performed.

In Fig. 13 and 15, we assumed the  $Z'$  couples with equal strength to the DM and leptons, i.e.  $g_\chi = g_\ell$ . If instead we take  $g_\chi > g_\ell$ , the constraints are relaxed and thus the allowed region of parameter space enlarged. This is illustrated in Fig. 14, in which we take  $g_\chi = 4g_\mu$  (left panel) and  $g_\chi = 8g_\mu$  (right panel). We see that increased  $g_\chi$  lowers the relic density curves. The LHC curves are independent of the choice of  $g_\chi$  when  $m_{Z'} < 2m_\chi$ ; for  $m_{Z'} > 2m_\chi$  the constraints on  $g_\ell$  become weaker as we enlarge  $g_\chi$ , due to the increased branching ratio of the  $Z'$  to invisible final states. In Figs. 13 and 14, this occurs for  $m_{Z'} > 20$  GeV, and we note an upturn in the LHC curves at that point. The LHC results for high  $Z'$  masses  $m_{Z'} > m_z$  have not been shown in Fig. 14, as they are weaker than the DD results.

The LHC curves shown in Fig. 13, 14 and 15 assume  $m_\chi = 10$  GeV. For other DM masses, the exclusion curves are approximately the same, except for a change to the point where  $m_{Z'} = 2m_\chi$ , beyond which the  $Z'$  is heavy enough for the dark branching ratio to be non-zero.<sup>3</sup>

## VIII. CONCLUSIONS

We have considered a leptophilic WIMP scenario in which DM does not couple to SM quarks at tree-level, and instead couples only to SM leptons. In this scenario, the DM has WIMP-scale interaction with leptons, accounting for the relic density, but suppressed signals in direct detection experiments and hadron colliders, consistent with the null results from these searches to date.

We explored such a leptophilic DM in the context of a simple  $Z'$  model, in which DM-lepton interactions are mediated by the exchange of a new vector boson which couples to one of the SM leptons flavours,  $\ell = e, \mu$ , or  $\tau$ , with Lorentz structure  $\Gamma_\chi \otimes \Gamma_\ell = V \otimes V$  or  $A \otimes V$ . DM-quark interactions are induced at loop level through kinetic mixing of the  $Z'$  and SM hypercharge, providing nuclear recoil signals in direct detection experiments.

Despite the loop-suppressed nature of this process, the resulting bounds are strong. For  $\Gamma_\chi \otimes \Gamma_\ell = V \otimes V$  the DD bounds eliminate all parameter space for which the correct relic density can be obtained, except if the DM annihilation cross section has a strong resonant enhancement. For  $\Gamma_\chi \otimes \Gamma_\ell = A \otimes V$  the direct detection cross section is velocity suppressed, resulting in weaker constraints, but even so the DD bounds eliminate significant parameter space. For DM coupling to muons, these bounds are comparable to those from  $(g-2)_\mu$ .

Production of leptophilic  $Z'$  at the LHC occurs via the radiation of a  $Z'$  from Drell-Yan leptons. We determined exclusion limits for the  $Z'$  mass and coupling strength, using results from a recent ATLAS analysis of  $pp \rightarrow Z \rightarrow 4e$  or  $4\mu$ , at  $\sqrt{s} = 8$  TeV and  $\mathcal{L} = 20.7$  fb<sup>-1</sup>. We also projected the future exclusion/discovery reach for  $\sqrt{s} = 14$  TeV and higher luminosities, for both low and high mass  $Z'$  bosons. For  $\ell = e, \mu$ , the combination of the LHC, direct detection, and relic density constraints excludes most parameter space, except that for which the DM annihilation at freezeout is resonantly enhanced. For  $\ell = \mu$ , some non-resonant parameter space remains open for  $m_\chi \gtrsim 200$  GeV, while for  $\ell = e$  this is eliminated by LEP-II bounds. For  $\ell = \tau$ , however, no LHC bounds exist, and much more parameter space is open.

In conclusion, despite the absence of tree-level interactions with quarks, this leptophilic dark matter model is strongly constrained by results from nuclear recoil and hadron collider experiments.

*Note added:* A recent paper has calculated limits on a  $Z'$  boson which couples to muon lepton number, based on neutrino trident production [59, 62]. These limits are a factor of  $\sim 5$  stronger than those from  $(g-2)_\mu$ .

## ACKNOWLEDGEMENTS

NFB, YC and AM were supported by the Australian Research Council and RKL by the Commonwealth of Australia.

- 
- [1] G. Jungman, M. Kamionkowski and K. Griest, Phys. Rept. **267**, 195 (1996).
  - [2] G. Bertone, D. Hooper and J. Silk, Phys. Rept. **405**, 279 (2005).
  - [3] L. Bergstrom, Rept. Prog. Phys. **63**, 793 (2000)
  - [4] XENON100 Collaboration, Phys. Rev. Lett. **109**, 181301 (2013) [arXiv:1207.5988 [astro-ph]].
  - [5] LUX Collaboration, Phys. Rev. Lett. **112**, 091303 (2014) [arXiv:1310.8214 [astro-ph]].

- [6] Q-H. Cao, E. Ma and G. Shaughnessy, Phys. Lett. B. **673**, 152 (2009) [arXiv:0901.1334 [hep-ph]].
- [7] A. Ibarra, A. Ringwald, D. Tran and C. Weniger, JCAP **0908**, 017 (2009) [arXiv:0903.3625 [hep-ph]].
- [8] D. Schmidt, T. Schwetz and T. Toma, Phys. Rev. D **85**, 073009 (2012) [arXiv:1201.0906 [hep-ph]].
- [9] P. Agrawal, Z. Chacko and C. Verhaaren (2014), [arXiv:1402.7369 [hep-ph]].
- [10] J. Kopp, L. Michaels and J. Smirnov (2014), [arXiv:1401.6457 [hep-ph]].
- [11] T. Cohen and K. Zurek, Phys. Rev. Lett. **104**, 101301 (2010) [arXiv:0909.2035 [hep-ph]].

<sup>3</sup> Even when  $Br(\text{DM})$  is non-zero, if  $g_\chi \sim g_\ell$  the cross section and thus the exclusion curves change only by a modest factor.

- [12] E. Baltz and L. Bergstrom, Phys. Rev. D **67**, 043516 (2003) [arXiv:hep-ph/0211325 [hep-ph]].
- [13] C-R. Chen and F. Takahashi, JCAP **0901**, 004 (2009) [arXiv:0810.4110 [hep-ph]].
- [14] D. Spolyar, M. Buckley, K. Freese, D. Hooper and H. Murayam (2009), [arXiv:0905.4764 [astro-ph]].
- [15] P. Ko and Y. Omura, Phys. Lett. B **701**, 363 (2011) [arXiv:1012.4679 [hep-ph]].
- [16] W. Chao, Phys. Lett. B **695**, 157 (2011) [arXiv:1005.1024 [hep-ph]].
- [17] M. Das and S. Mohanty (2013), [arXiv:1306.4505 [hep-ph]].
- [18] P. Schwaller, T. Tait and R. Vega-Morales (2013), [arXiv:1305.1108 [hep-ph]].
- [19] P. Fox and E. Poppitz, Phys. Rev. D **79**, 083528 (2009) [arXiv:0811.0399 [hep-ph]].
- [20] J. Kopp, V. Niro, T. Schwetz and J. Zupan, Phys. Rev. D **80**, 083502 (2009) [arXiv:0907.3159 [hep-ph]].
- [21] X-J. Bi, X-G. He and Q. Yuan, Phys. Lett. B **678**, 168 (2009) [arXiv:0903.0122 [hep-ph]].
- [22] Y. Bai and J. Berger (2014), [arXiv:1402.6696 [hep-ph]].
- [23] M. Ackermann et al. (Fermi LAT Collaboration), Phys. Rev. D **89**, 042001 (2014) [arXiv:1310.0828 [hep-ph]].
- [24] O. Adriani et al., Phys. Rev. Lett. **111**, 081102 (2013)
- [25] M. Ackermann et al. (Fermi LAT Collaboration), Phys. Rev. Lett. **108**, 011103 (2012)
- [26] M. Aguilar et al. (AMS Collaboration), Phys. Rev. Lett. **110**, 141102 (2013)
- [27] D. Hooper, P. Blasi and P. Serpico, JCAP **0901**, 025 (2009) [arXiv:0810.1527 [astro-ph]].
- [28] S. Profumo, Cent. Eur. J. Phys. **10**, 1 (2011) [arXiv:0812.4457 [astro-ph]].
- [29] M. Kachelriess, P.D. Serpico and M.Aa. Solberg, Phys. Rev. D **80**, 123533 (2009) [arXiv:0911.0001 [hep-ph]].
- [30] P. Fox, R. Harnik, J. Kopp and Y. Tsai, Phys. Rev. D **84**, 014028 (2011) [arXiv:1103.0240 [hep-ph]].
- [31] CMS Collaboration, JHEP **09**, 01 (2012) [arXiv:1206.5663 [hep-ex]].
- [32] ATLAS Collaboration, Phys. Rev. Lett. **110**, 011802 (2013)
- [33] Y. Bai and T. Tait, Phys. Lett. B **723**, 384-387 (2013)
- [34] L. Carpenter, A. Nelson, C. Shimmin, T. Tait and D. Whiteson, (2011) [arXiv:1212.3352 [hep-ex]].
- [35] N. Bell, J. Dent, A. Galea, T. Jacques, L. Krauss and T. Weiler, Phys. Rev. D **86**, 096011 (2012) [arXiv:1209.0231 [hep-ph]].
- [36] ATLAS Collaboration, (2014) [arXiv:1404.0051 [hep-ex]].
- [37] ATLAS Collaboration, Phys. Rev. Lett. **112**, 041802 (2013)
- [38] R. Foot, Mod. Phys. Lett. A **06**, 527 (1990).
- [39] X.G. He, G. Joshi, H. Lew and R. Volkas, Phys. Rev. D **43**, 22 (1991).
- [40] X.G. He, G. Joshi, H. Lew and R. Volkas, Phys. Rev. D **44**, 2118 (1991).
- [41] S. Baek and H. Ko, JCAP **0910**, 011 (2009) [arXiv:0811.1646 [hep-ph]].
- [42] D. Christensen and C. Duhr, Comput.Phys.Commun. **180**, 1614 (2009) [arXiv:0806.4194 [hep-ph]].
- [43] G. Blanger, F. Boudjema, A. Pukhov and A. Semenov, (2013) [arXiv:1305.0237 [hep-ph]].
- [44] P. Ade et al. (Planck Collaboration), (2013) [arXiv:1303.5076 [hep-ph]].
- [45] B. Holdom, Phys. Lett. B **166**, 196 (1986)
- [46] K.S. Babu, C. Kolda, J. March-Russell, Phys. Rev. D **57**, 6788 (1998) [arXiv:hep-ph/9710441].
- [47] A. Hook, E. Izaguirre and J. G. Wacker, (2010) [arXiv:1006.0973 [hep-ph]].
- [48] P. Fayet, Phys. Rev. D **75**, 115017 (2007) [arXiv:hep-ph/0702176].
- [49] J. Beringer et al. (Particle Data Group), Phys. Rev. D **86**, 010001 (2012)
- [50] L. Auerbach et al., Phys. Rev. D **63**, 112001 (2001) [arXiv:hep-ex/0101039].
- [51] The LEP Collaborations, (2003) [arXiv:hep-ex/0312023].
- [52] M. Buckley, D. Hooper, J. Kopp and E. Neil, Phys. Rev. D **83**, 115013 (2011) [arXiv:1103.6035 [hep-ph]].
- [53] CMS Collaboration (2013) [arXiv:1210.3844 [hep-ex]].
- [54] ATLAS Collaboration (2014) [arXiv:1403.5657 [hep-ex]].
- [55] J. Alwall, M. Herquet, F. Maltoni, O. Mattelaer, T. Stelzer, (2011) [arXiv:1106.0522 [hep-ph]].
- [56] T. Sjstrand, S. Mrenna and P. Skands, Comput.Phys.Commun. **178**, 852 (2008) [arXiv:0710.3820 [hep-ph]].
- [57] J. Conway et al., <http://www.physics.ucdavis.edu/conway/research/software/pgs/pgs4-general.htm>, Accessed July 2014.
- [58] E. Conte, B. Fuks and G. Serret, Comput.Phys.Commun. **184**, 222 (2013) [arXiv:1206.1599 [hep-ph]].
- [59] W. Altmannshofer, S. Gori, M. Pospelov and I. Yavin, (2014) [arXiv:1403.1269 [hep-ph]].
- [60] K. Harigaya, T. Igari, M. Nojiri, M. Takeuchi and K. Tobe, (2013) [arXiv:1311.0870 [hep-ph]].
- [61] ATLAS Collaboration Eur. Phys. J. **C72**, 1909 (2012) [arXiv:1110.3174 [hep-ex]].
- [62] W. Altmannshofer, S. Gori, M. Pospelov and I. Yavin, (2014) [arXiv:1406.2332 [hep-ph]].